An acetoacetate-inducible bacterial sensor

David T. Gonzales[1], Tanel Ozdemir[1], Geraint M. Thomas[1]
and Chris P. Barnes[1,2,*]

[1] Department of Cell and Developmental Biology, University College London, London, UK
[2] Department of Genetics, Evolution and Environment, University College London, London, UK
*To whom correspondence should be addressed. Email: christopher.barnes@ucl.ac.uk

Abstract

Whole cell biosensors have great potential to be used as diagnostic and treatment tools in biomedical applications. Bacterial biosensors that respond to specific metabolites can help analyze spatio-temporal gradients in the body or cue expression of therapeutic agents in diseased sites. In this study, we developed an acetoacetate bacterial sensor by inserting the promoter of the atoSC two-component system (TCS) into a promoterless GFP expression plasmid and transformed it into *E. coli* DH5α and *E. coli* Nissle 1917, which both contain the atoSC TCS. This bacterial biosensor has a dynamic range of 0.01-1mM of acetoacetate, which is within the range of physiological concentrations in the blood, and exhibits up to a 100-fold change of induced GFP expression as measured by relative fluorescence. Comparing combinations among the two host strains and high/low-copy plasmid variations of the biosensor, we observed the fastest and highest response to acetoacetate with the *E. coli* Nissle 1917 low copy plasmid biosensor. Induction experiments on the biosensor using 50mM of the short chain fatty acids (SCFA) acetate, proprionate, and butyrate showed no response, indicating its specificity between acetoacetate and SCFAs. This acetoacetate bacterial sensor is a valuable contribution to the library of biosensors that may eventually be used for *in vivo* clinical applications.

keywords: atoSC two-component system, synthetic biology, whole cell biosensor

1 Introduction

Natural sensing systems in bacteria detect external signals in the environment and relay these into the cell for appropriate responses. As an integral part of a complex biological system, these have evolved to be sensitive, specific, and robust, making them attractive to harness for technological applications. In the field of synthetic biology, bacteria are engineered into whole cell biosensors by combining three parts: (i) a membrane-bound or cytoplasmic sensor to detect the signal, (ii) an internal circuit to process signals, and (iii) an actuator to transduce the processed signal into an output [1]. Sensors can come in the form of two-component systems (TCS), cytoplasmic regulatory proteins, RNA riboswitches, and other environment-responsive sensors [2]. Whole cell biosensors can be used to detect harmful substances in the environment or monitor key metabolites in bioprocessing units. When the sensor is linked to fluorescence expression, real-time information of the system can be obtained quickly and inexpensively through flow cytometry [3]. In addition, biosensors can be integrated directly to metabolic pathways to control and regulate enzyme expression to improve titer yields [4]. For medical applications, whole cell biosensors can provide non-invasive and targeted therapeutic strategies when incorporated with sensors that respond to metabolites or conditions in diseased sites of the body [5, 6]. Although many challenges and limitations still remain for whole cell biosensors [7], the growing number, and improved methods in assembling internal genetic circuits, will help their translation into clinical applications.

In the present study, we developed and characterized an acetoacetate biosensor in *E. coli*. Acetoacetate is one of the three ketone bodies (acetone, acetoacetate, and β-hydroxybutyrate) produced in the liver. It serves as an alternative source of energy that is distributed through the bloodstream at concentrations between 0.02-3.0mM [8, 9, 10] when glucose levels are low. Ketone bodies also confer protective effects to the brain, which is why the ketogenic diet (high fat-low carbohydrate) is used to induce ketosis as a method of treatment against epilepsy [11]. However, excess ketone bodies accumulated in the blood from prolonged starvation, diabetes (lack of insulin), or excessive alcohol consumption can result in ketoacidosis [12], a harmful and extreme form of ketosis. Ketone body levels, in the form of acetoacetate or β-hydroxybutyrate, are monitored in urine and blood in diabetic patients to help control blood glucose and reduce incidence of complications. Ketone bodies are also monitored in the blood and milk of cows, who are susceptible to ketosis during pregnancy and can adversely affect health and milk production [13]. While strip tests reacting sodium nitroprusside with acetoacetate will likely be easier and cheaper in terms of blood and urine diagnostics, biosensors can be applied into more complex, fine scale, and real-time applications such as monitoring acetoacetate levels in the liver and gut to provide important information on the dynamics and spatial patterns of acetoacetate metabolism. For example, bacterial biosensors that can colonize tissues and microenvironments *in vivo* have already been demonstrated in the rat liver to detect tumors [5] and in the rhizosphere of plants to detect nitrate availability [14]. Bacterial biosensors that contain trigger and memory elements have also been developed in murine gut derived *E. coli* to show how genetic circuits can be used to monitor the complex gut environment [15].

We developed the whole cell biosensor using the atoSC two-component system, which is triggered by acetoacetate and is responsible for activating the genes necessary for short chain fatty acid (SCFA) and acetoacetate metabolism, poly-(R)-3-hydroxybutyrate biosynthesis, and chemotaxis in *E. coli* [16, 17, 18, 19]. The atoSC two-component system is composed of a membrane-bound homodimeric histidine kinase sensor, atoS, which detects acetoacetate in the environment and auto-phosphorylates. AtoS then passes on the phosphoryl group to atoC, which dimerizes and binds onto the two 20bp palindrome stretches (*Pato*) upstream the atoDAEB operon to promote σ-54-dependent transcription [16, 20, 21, 22, 23] (Fig. 1). To construct the acetoacetate biosensor, the *Pato* promoter region was inserted into a high-copy promoterless GFP expression plasmid and transformed into *E. coli* DH5α, which contains the atoSC two-component system within its genome. Characterisation experiments were performed to determine the dynamic range of acetoacetate concentration and fold-change expression of GFP in the biosensors. These experiments were monitored through the plate reader to obtain growth curves and normalized fluorescence time courses, and through flow cytometry to obtain fluorescence intensity population distributions of the induced cultures. The whole cell biosensor was shown to be able to detect acetoacetate in a range of 0.01-1mM and exhibit up to a 100-fold change in induced GFP expression. Additionally, we demonstrated the sensor to work in a low-copy plasmid and in *E. coli* Nissle 1917, a human probiotic strain which has been widely used in clinical settings and microbiome engineering studies [24, 25, 26, 27].

2 Materials and Methods

2.1 Bacterial strains and media

The bacterial strains and plasmids used in this study are listed in Table 1. Both *E. coli* DH5α and *E. coli* Nissle 1917 were confirmed to carry the atoSC two-component system by PCR (Fig. S1). Primers used were developed from a whole genome assembly of *E. coli* DH5α [28]. All bacterial cultures were carried out in 5ml liquid Luria-Bertani (LB) broth and incubated at 37°C and 180rpm in a shaking incubator. Antibiotics were added at a final concentration of 50μg/ml kanamycin when indicated. Media was supplemented with acetoacetate, in the form of H_2O dissolved lithium acetoacetate (Sigma-Aldrich), during acetoacetate induction experiments. Chemically competent cells for all bacterial strains were prepared by $CaCl_2$ method and then stored at -80°C until used for chemical transformation.

2.2 Construction of plasmids

OG241 (Oxford Genetics), a pUC high-copy (500-700 copies/cell) promoterless GFP expression plasmid, was used as a backbone plasmid for the *Pato* promoters. Different variations of promoters were PCR amplified and extended with restriction enzyme sites from the genomic DNA of *E. coli* DH5α and inserted upstream the GFP gene to the multiple cloning site (MCS) of OG241 by restriction enzyme digest and ligation (Figs. S2-4). PatoG-OG241 contains the *Pato* promoter region up until the start codon of *atoD* to continue in-frame with GFP. PatoK-OG241 is the same as PatoG-OG241 except that the GFP is out of frame with the start codon. PatoL-OG241 contains the *Pato* promoter region up until before the probable native ribosomal binding site (RBS) and continues with Bba_B0034, a strong RBS from the iGEM registry (www.parts.igem.org), and then the start codon of GFP. Oxb19-OG241 contains a strong constitutive promoter, Oxb19 (Oxford Genetics), upstream of GFP. All promoter regions of the plasmids were confirmed by capillary sequencing. Low copy versions of plasmids OG241, Oxb19-OG241, PatoL-OG241, and PatoM-OG241 were made by switching the pUC origin of replication region with SC101, a low-copy (2-5 copies/cell) origin of replication (Figs. S5-6). These plasmids were labeled as LOG241, for low copy OG241. The plasmids were then transformed into *E. coli* DH5α and *E. coli* Nissle 1917 for growth and induction experiments. Further details are documented in the Supplementary Material. Plasmids are available at Addgene (www.addgene.org, Plasmid IDs 72838-72842 for the high-copy plasmids and 72844-72848 for the low-copy plasmids).

2.3 Growth curves and flow cytometry induction assays

The plasmid transformed bacteria were cultured in 5ml LB broth with 50μg/ml kanamycin overnight (12 hours) at 37°C and then diluted 1:100(v/v) into fresh 5ml LB broth with 50μg/ml kanamycin. The diluted cultures were incubated for 1 hour and then induced with varying concentrations of acetoacetate (0mM, 1e^{-3}mM, 1e^{-2}mM, 1e$^{-1.5}$mM, 1e^{-1}mM, 1e$^{-0.5}$mM, 1mM, and 10mM). After induction, 200μl of the cultures are aliquoted into a clear bottom, black walled 96-well plate (Grenier), sealed with a gas permeable membrane, and placed into a plate reader (BMG FUOstar OPTIMA). The plate reader was set at 37°C with shaking (150rpm, 4mm double orbital), absorbance (540nm), and fluorescence (480nm excitation, 520nm emission) readings every 10 mins. The gain used for fluorescence readings was 2,000 and all plate reader readings were taken by 3mm diameter orbital averaging. The remainder of the induced cultures were incubated further for 15 hours for flow cytometry analysis. flow cytometry samples were prepared by pelleting 50μl of the cultures by centrifuge (1 min, 13,000XG), aspirating out the supernatant, washing with 500μl phosphate-buffered saline solution (PBS), and then resuspending in fresh 500μl PBS. Samples were analyzed on a flow cytometer (BD Acuri C6, 22μm core) using the slow mode (14μl/min) to record FL1 filter readings (533/30nm for GFP) for 10,000 events. For time series experiments, flow cytometry samples were aliquoted, prepared, and analyzed from the incubating cultures every 1 hour. All samples were done in triplicate from the bacterial colony used for initial culture.

2.4 Data analysis

Growth curve results were processed by taking the natural logarithm of the absorbance values and plotting ln(OD_{540}) against time. Relative fluorescence units (RFU) values were normalized by dividing with OD_{540}. Ratios of normalized RFU values of induced and uninduced cultures were used to compare the induction responses of the different strains and plasmid copies over time in the plate reader. Growth curves were modelled using a modified version of the Gompertz model [30, 34]

$$\ln \mathrm{OD}_{540}(t) = \ln N_0 + K \exp\left[-\exp(\frac{\mu e}{K}(\lambda - t) + 1)\right],$$

where N_0 is the initial optical density, K is the carrying capacity, μ is the maximal growth rate and λ is the lag phase time. Flow cytometry characterisation curves were created by plotting

the density of $\log_{10}$(no. of events) vs. fluorescence intensity, $\log_{10}$ (relative fluorescent units, RFU). Characterisation curves were modelled using a Hill function

$$I = P_{min} + (P_{max} - P_{min})\frac{\left(\frac{[X]}{K_d}\right)^n}{1 + \left(\frac{[X]}{K_d}\right)^n},$$

where I is the median RFU, $[X]$ is the concentration of acetoacetate and P_{min}, P_{max}, K_d and n are the minimum fluorescence, maximum fluorescence, dissociation constant, and Hill coefficient, respectively. Both models were initially fit using maximum likelihood followed by a Bayesian analysis using Markov chain Monte Carlo (MCMC) [35] in the R statistical software environment [36]. Further details of the model fitting are provided in the Supplementary Material.

3 Results

3.1 Induction of high-copy plasmids in *E. coli* DH5α

Initially, the biosensors were tested for inducibility at 0mM and 10mM acetoacetate. *E. coli* DH5α and *E. coli* DH5α harboring OG241 and PatoK-OG241 showed no GFP expression by acetoacetate induction. *E. coli* DH5α harboring Oxb19-OG241 constitutively expressed GFP. *E. coli* DH5α harboring the plasmids PatoG-OG241, PatoL-OG241, and PatoM-OG241 were observed to be acetoacetate inducible (Fig. S8). Growth curves and specific growth rate (μ) distributions showed no apparent difference that could be caused by the additional carbon source from acetoacetate. *E. coli* DH5α harboring PatoL-OG241 was also used to test induction by short chain fatty acids acetate, proprionate, and butyrate, but showed no induction at 50mM for each SCFA (Fig. S10).

3.2 Dynamic range of high-copy plasmids in *E. coli* DH5α

The dynamic ranges of the *E. coli* DH5α with high copy PatoG-OG241, PatoL-OG241, and PatoM-OG241 were determined by acetoacetate induction at concentrations between 0mM and 10mM. GFP expression was induced starting after $1e^{-2}$mM acetoacetate for all three biosensors and was saturated at $1e^{-0.5}$mM for PatoG-OG241 (Fig. 3A) and 1mM acetoacetate for both PatoL-OG241 (Fig. 3C) and PatoM-OG241. Within their dynamic ranges, GFP expression, as measured by RFU intensity, increased >100-fold for PatoG-OG241 and >10-fold for PatoL-OG241 and PatoM-OG241. Hill function fits (Figs. 3B, 3D, and S27-29) showed that the medians of the parameters P_{min}, P_{max}, K_d and n were 708.90, 13,749.18, 0.159, and 2.832 for PatoG-OG241, 557.42, 4,598.02, 0.221, and 1.684 for PatoL-OG241, and 589.67, 2,855.60, 0.228, and 1.639 for PatoM-OG241 in *E. coli* DH5α, respectively.

3.3 Induction and temporal response of low-copy plasmids in *E. coli* DH5α

Low-copy versions of the OG241, Oxb19-OG241, PatoL-OG241, and PatoM-OG241 biosensors were constructed using LOG241 (SC101 origin of replication) in place of OG241 as the backbone plasmid. The PatoL-LOG241 and PatoM-LOG241 in *E. coli* DH5α biosensors also showed inducibility with acetoacetate, but was observed to have a heterogeneous population with respect to fluorescence intensity (Figs. 4B and S8K-L) as compared to the high-copy version (Figs. 4A and S8E-F). The time series of induced cultures showed that the high-copy PatoL-OG241 in *E. coli* DH5α had one homogeneous population shifting in fluorescence intensity from 3-16 hours (Fig. 4A). On the other hand, the low-copy PatoL-LOG241 in *E. coli* DH5α showed two separate populations at low and high fluorescence intensity. Along the succeeding hours after induction, the low fluorescence population decreases while the higher fluorescence population increases. Additionally, similar to the high-copy PatoL-OG241, there is an observed general shifting towards higher fluorescence in the low-copy PatoL-LOG241 (Fig. 4B).

3.4 *E. coli* Nissle 1917 acetoacetate sensors

PatoL-OG241 and PatoL-LOG241 plasmids transformed into *E. coli* Nissle 1917 also exhibited acetoacetate inducibility. Growth curves for both plasmids in *E. coli* Nissle 1917 (Figs. 5A & 5C) reached their stationary phases in a shorter amount of time and specific growth rates were higher as compared to *E. coli* DH5α strains (Figs. 2A & 2C). Specific growth rate (μ) medians of PatoL-OG241 in *E. coli* Nissle 1917 for uninduced and induced cultures were 0.00527 and 0.00438, respectively. Specific growth rate (μ) medians of PatoL-LOG241 in *E. coli* Nissle 1917 for uninduced and induced cultures were 0.00424 and 0.00341, respectively (Figs. 5A, 5C, S23-26). While the *E. coli* DH5α with PatoL-OG241 biosensors had a specific growth rate (μ) of 0.00164 and 0.00184 and *E. coli* DH5α with PatoL-LOG241 biosensors had a specific growth rate (μ) of 0.000972 and 0.000990 for uninduced and 10mM acetoacetate induced treatments, respectively (Figs. 2C, S15-16 and S19-20). The low-copy PatoL-LOG241 plasmid in *E. coli* Nissle 1917 also resulted in a heterogeneous population (Fig. 5D and S9F) similar to the low-copy biosensors in *E. coli* DH5α. In both cases of host strains, the high-copy plasmid resulted in a higher fold change of induction.

Induced/uninduced ratios of normalized RFU vs. time plots describe the response of the bacterial biosensors in culture to the acetoacetate inducer. Comparing the high-copy PatoL-OG241 (Fig. 6A) and low-copy PatoL-LOG241 (Fig. 6B) implementations in *E. coli* DH5α, the low-copy biosensor results in larger standard deviations for the replicates. In *E. coli* Nissle 1917, the low-copy PatoL-LOG241 biosensor (Fig. 6D) results in a faster time to a maximum RFU induction ratio as compared to the high-copy biosensor PatoL-OG241 (Fig. 6C).

4 Discussion

We constructed a whole bacterial cell biosensor for acetoacetate and demonstrated it to specifically respond to concentrations of acetoacetate within its physiological range in human blood. The biosensor had a dynamic range between 0.01mM to 0.10mM for PatoG-OG241 and 0.01mM to 1.0mM for PatoL-OG241 and PatoM-OG241 in *E. coli* DH5α. Physiological acetoacetate concentrations in human blood ranges in between 0.02-3mM [8, 9, 10]. The use of the entire native *Pato* region until the start codon of the *ato* operon in PatoG-OG241 showed a greater response in fluorescence output as compared to the PatoL-OG241 and PatoM-OG241 biosensors by approximately 10-fold (Figs. 3A, 3C, and S27-29). This may be due to transcriptional or translational regulatory mechanisms because PatoL-OG241 and PatoM-OG241 differ with PatoG-OG241 only between their transcriptional start site and the start codon, including the RBS. The median magnitudes of the Hill coefficient (n), representing the cooperativity of the system, are lower for PatoL-OG241 (1.684) and PatoM-OG241 (1.639) compared to PatoG-OG241 (2.832) in *E. coli* DH5α. The lower Hill coefficients result in a wider dynamic range against acetoacetate induction concentrations. The different behaviors resulting from biosensor variations show how sequence elements can alter the properties of the biosensor. These variations can be used to adjust the dynamic range or response output of the sensor appropriate for the application.

Although the atoSC two-component system induces the *atoDAEB* operon necessary for SCFA metabolism, the acetoacetate bacterial biosensor was specific towards acetoacetate only and not acetate, proprionate, or butyrate at concentrations of 50mM (Fig. S10). This is in agreement to previous studies that linked acetoacetate as the inducer of the atoDAEB operon. Wild type *E. coli* was observed to be able to grow on acetoacetate as a sole carbon source, but not with SCFAs. However, the mutant *E. coli* strain containing $atoC^{c}$, which caused constitutive expression of the *atoDAEB* operon, was able to grow on butyrate as a sole carbon source [17, 18] - indicating that the atoSC two-component system is one of the regulatory mechanisms for SCFA metabolism. Spermidine was also observed to increase poly-(R)-3-hydroxybutyrate synthesis, which is regulated by the atoSC two-component system and the *atoDAEB* operon. However, whether spermidine directly phosphorylates atoS in a similar manner to acetoacetate, or one of its metabolic products somehow influences the atoSC two-component system, is unknown [31]. The acetoacetate biosensor developed in this study could be used to further investigate the

mechanism of spermidine on the the atoSC two component system.

Induction experiments of high and low copy biosensors showed a difference of population fluorescence heterogeneity. In *E. coli* DH5α, the high copy PatoL-OG241 biosensor had one homogeneous population throughout induction (Figs. 4A & 5B) and the low copy PatoL-LOG241 plasmid had two distinct subpopulations with either low or high fluorescence (Figs. 4B & 5D). In the low copy biosensor, the low fluorescence population decreased and the high fluorescence population increased as time after induction progressed. These subpopulations could be a result of the competition for the transcription factor atoC between the two *Pato* promoters present in the GFP expression plasmid and the genome of *E. coli*. In high copy plasmids, the probability of a phosphorylated atoC binding onto the *Pato* promoter on PatoL-OG241, as compared to the genomic *Pato*, is much higher. A similar heterogeneous behavior in a low copy reporter plasmid was also observed in an arabinose-inducible bacterial sensor where a copy of the inducible system was also present in the chromosome of the host *E. coli*. This resulted in two distinct subpopulations of induced cells, as opposed to the homogeneous population observed in the arabinose transport-deficient strains harboring the reporter plasmid [32].

The acetoacetate sensor worked in both *E. coli* DH5α and *E. coli* Nissle 1917 but performed differently on each host and plasmid vector. Growth rates of *E. coli* DH5α were slow due to mutations in its genome that cause inferior growth phenotypes [33]. Median specific growth rates (μ) ranged between 0.0014-0.0022 for *E. coli* DH5α while 0.0035-0.0053 for *E. coli* Nissle 1917. The slow growth rate of *E. coli* DH5α affects the response time of the biosensor on acetoacetate, which begins to have significant induced GFP expression at the exponential phase up until the stationary phase. *E. coli* Nissle 1917 grows faster and reaches its stationary phase more quickly. The high copy plasmid in *E. coli* DH5α had a more apparent rise in normalized RFU ratios between induced and uninduced cultures as compared to its low copy strain (Figs. 6A & 6B), while the low copy plasmid in *E. coli* Nissle 1917 exhibited a faster increase of normalized RFU ratio compared to the high copy strain (Figs. 6C & 6D).

This acetoacetate bacterial sensor is a valuable addition to the steadily growing library of biosensors. Whole cell biosensors will eventually be able to help open up research opportunities to monitor biological systems, whether in an industrial microbiology setting or within *in vitro* and *in vivo* biomedical applications. The gut environment is of special interest for whole cell biosensors to monitor gut health. Stable populations of bacteria can be established in the gut microbiota and be used for long term diagnostics of specific metabolites in the gastrointestinal tract [6, 15].

Table 1: *E. coli* strains and plamids used in this study.

Strain or plasmid	**Description**	**Source**
E. coli		
DH5α	$F^-\phi 80lacZ\Delta M15\Delta(lacZYA\text{-}argF)U169recA1$ $endA1hsdR17(r_k^-,m_k^+)phoAsupE44thi\text{-}1gyrA96$ $relA1\lambda^-$; Competent cells for plasmid transformation.	Invitrogen
Nissle 1917	Widely-used probiotic; Also known as Mutaflor®.	*
Plasmids**		
OG241	High copy pUC derived from pBR322; KanR; 4540bp; Promotorless GFP expression plasmid with multiple cloning site (MCS) upstream GFP.	Oxford Genetics
Oxb19-OG241	Same as OG241 with a constitutive promoter; + control.	This study
PatoG-OG241	OG241 + promoter (*Pato* region including start codon); In-frame with GFP.	This study
PatoK-OG241	OG241 + promoter (*Pato* region including start codon); Out-of-frame with GFP; - control.	This study
PatoL-OG241	OG241 + promoter (*Pato* region with a strong ribosomal binding site).	This study
PatoM-OG241	OG241 + promoter (*Pato* region with a strong ribosomal binding site).	This study

*Kindly provided by Prof. Ian Henderson, University of Birmingham.

**Low copy versions of the plasmids OG241, Oxb19-OG241, PatoL-OG241, and PatoM-OG241 were also made by changing the high copy pUC origin of replication region with a low copy SC101 and labeled with LOG241 instead of OG241.

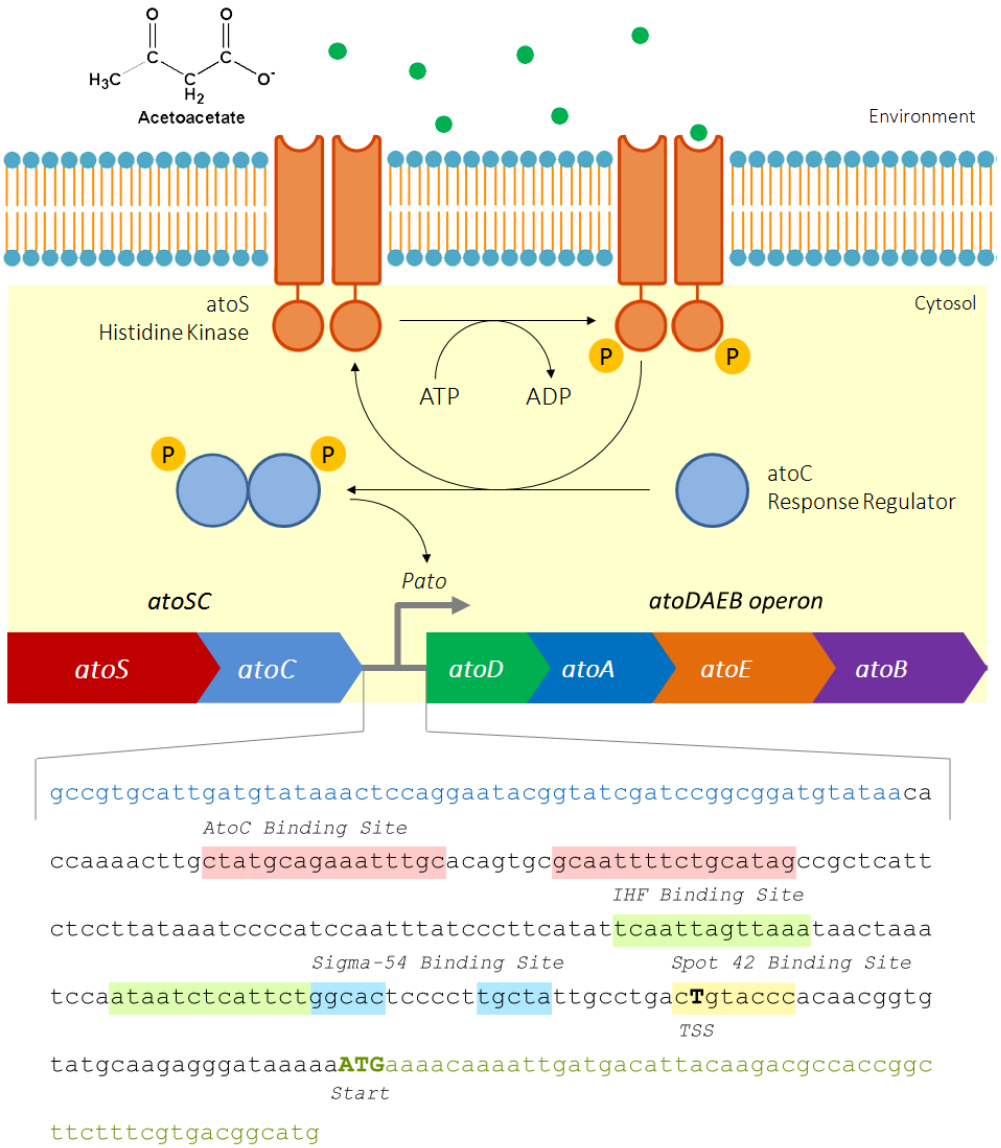

Figure 1: AtoSC two-component system in *E. coli*. Acetoacetate in the environment is detected by the membrane-bound homodimeric histidine kinase (atoS) and autophosphorylates. The phosphoryl group of atoS is passed on to the response regulator (atoC). The activated dimerized atoC acts as the transcriptional activator to the *ato* operon promoter *Pato* and activates expression of the *atoDAEB* operon. The *Pato* is a palindromic *atoC* binding site for the phosphorylated atoC. Two sequence stretches downstream *Pato* bear homology to integration host factor (IHF) binding sites, which were found to be necessary for atoC-mediated induction of the atoDAEB operon from expression experiments using wild type and IHF-negative *E. coli* mutants. The IHF sites allow optimal contact of the ELE-bound NtrC-type transcription factor with the adjacent promoter-bound σ-54 RNA polymerase [20]. Downstream the IHF sites, Spot 42 overlaps the transcription start site (TSS), which can inhibit expression when bound with a small regulatory RNA [29].

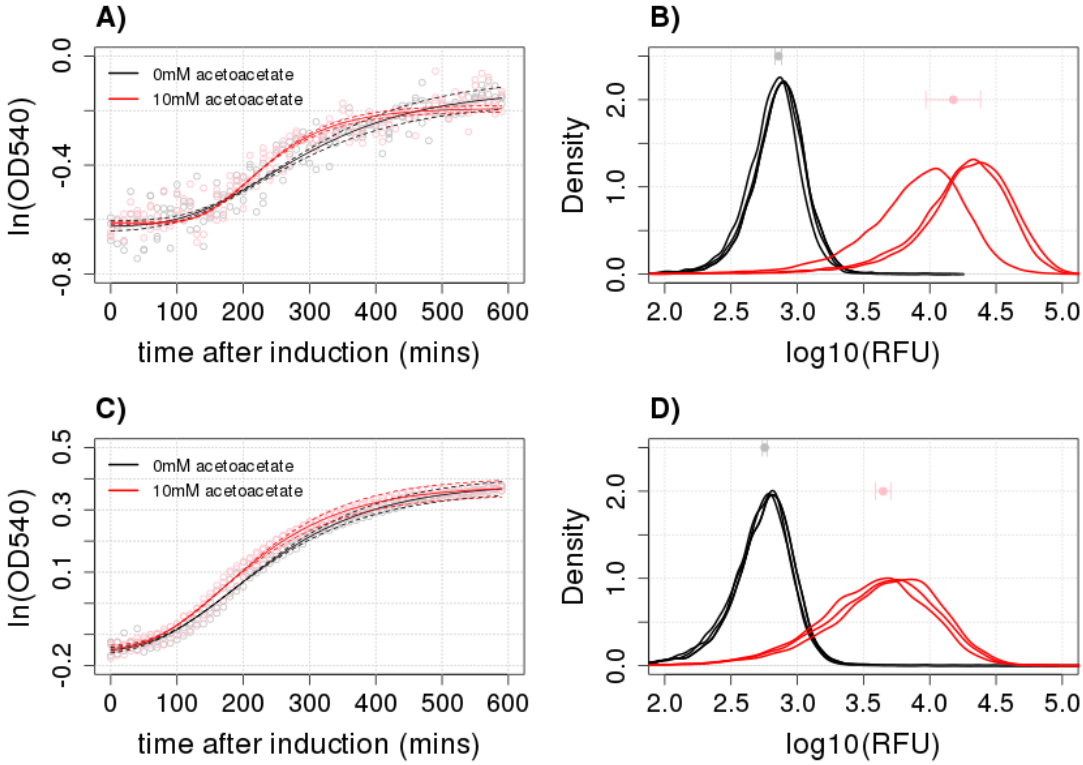

Figure 2: Acetoacetate-inducible bacterial sensors in *E. coli* DH5α. Growth curves with their 95% credible regions fitted using the Gompertz model are shown for PatoG-OG241 in *E. coli* DH5α (A) and PatoL-OG241 in *E. coli* DH5α (C). Median values from the posteriors of the specific growth rates are 0.0014 and 0.0022 for uninduced and induced PatoG-OG241 in *E. coli* DH5α, and 0.0017 and 0.0018 for uninduced and induced PatoL-OG241 in *E. coli* DH5α, respectively. Flow cytometry showed that the bacterial biosensors exhibited acetoacetate inducibility by an increase in $\log_{10}$(RFU) of >100-fold for PatoG-OG241 in *E. coli* DH5α (B) and >10-fold for PatoL-OG241 in *E. coli* DH5α (D) after 16 hours in culture compared to uninduced cultures.

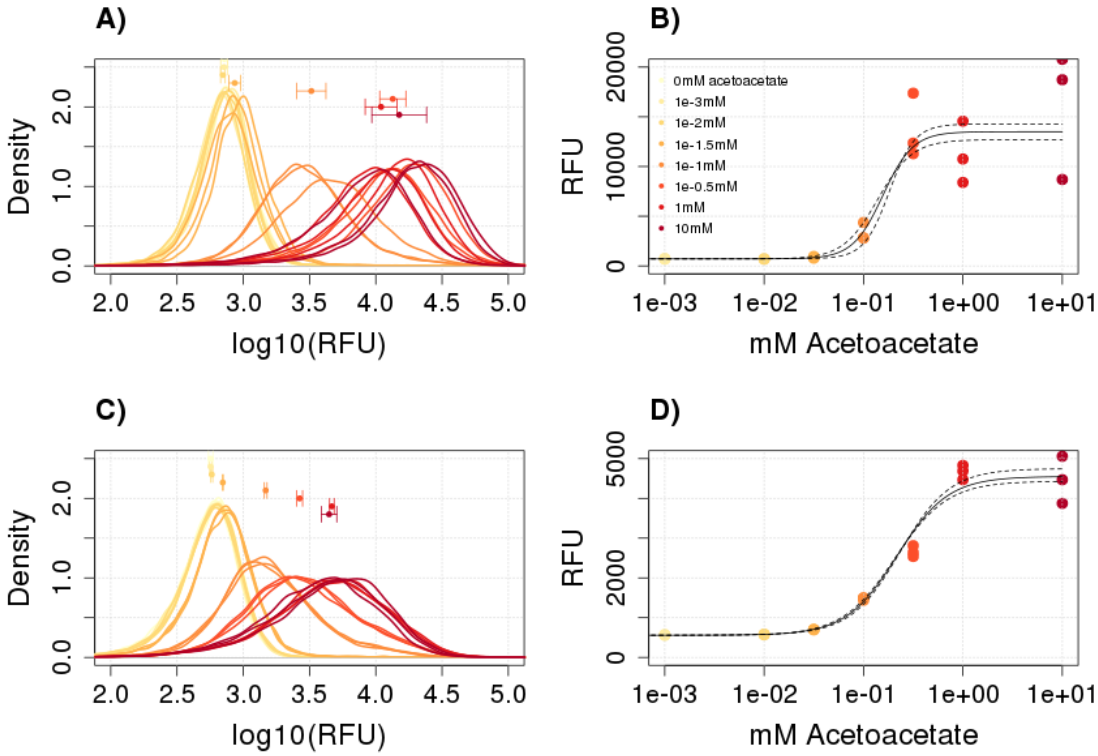

Figure 3: The dynamic ranges of PatoG-OG241 and PatoL-OG241 in *E. coli* DH5α. Flow cytometry density plots of PatoG-OG241 in *E. coli* DH5α (A) and its characterisation curves (B) show a dynamic range between 0.01mM to 1e-0.5mM with a corresponding >100-fold change in RFU. Flow cytometry density plots of PatoL-OG241 in *E. coli* DH5α (C) and its characterisation curves (D) show a dynamic range between 0.01mM to 1mM acetoacetate with a corresponding >10-fold change in RFU. Hill function models (with 95% credible regions) are fitted with the characterization plots to obtain parameter distributions for P_{min}, P_{max}, K_d, and n. Median values of the posteriors for the parameters are 709.05, 12931.22, 0.15, 2.88 and 557.59, 4600.51, 0.23, 1.64 for PatoG-OG241 and PatoL-OG241 in *E. coli* DH5α, respectively

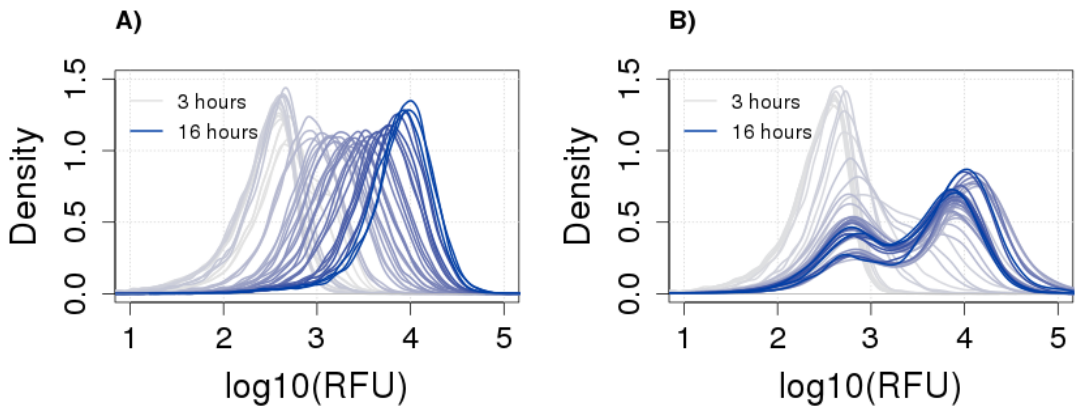

Figure 4: Induction time series of (A) PatoL-OG241 (high copy) and (B) PatoL-LOG241 (low copy) plasmids in *E. coli* DH5α. The biosensors were induced with 10mM of acetoacetate at the 3 hour mark and monitored up to 16 hours (grey to blue) at every hour by flow cytometry. The high copy plasmid exhibited a single population increasing its fluorescence intensity, while the low copy plasmid exhibited two populations shifting from low RFU intensity to high RFU intensity.

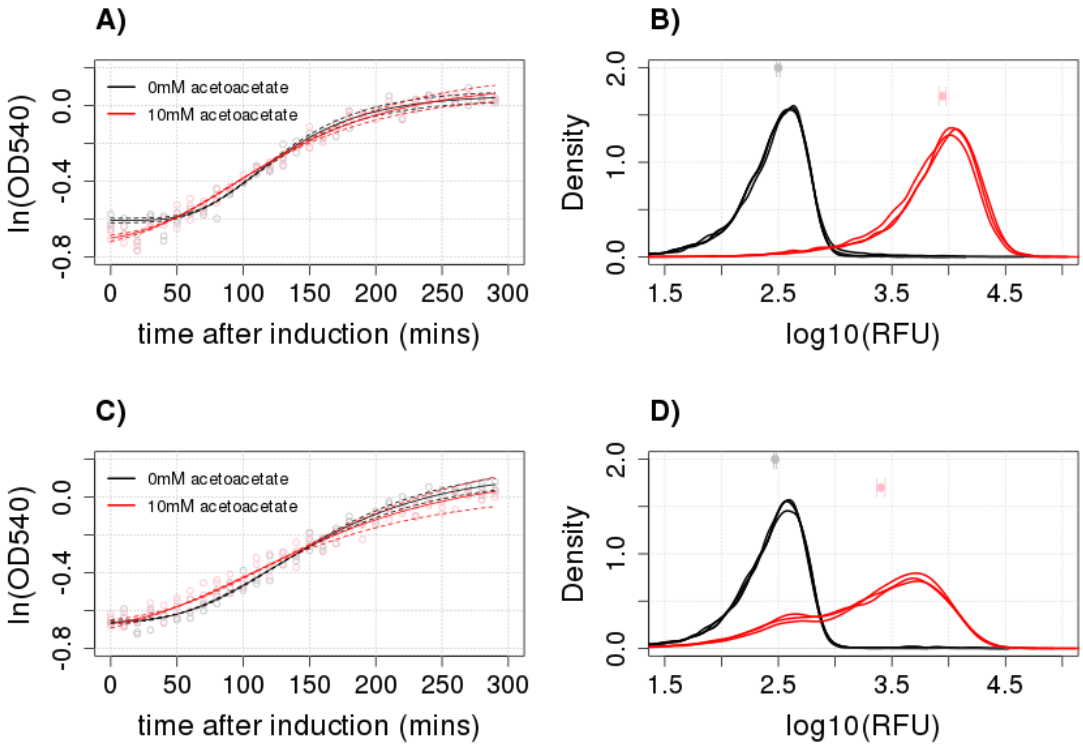

Figure 5: Induction of PatoL-OG241 (high copy) and PatoL-LOG241 (low copy) plasmids in *E. coli* Nissle 1917. Growth curves with their 95% credible regions fitted using the Gompertz model are shown for PatoL-OG241 in *E. coli* Nissle 1917 (A) and PatoL-LOG241 in *E. coli* Nissle 1917 (C). Median values from the posteriors of the specific growth rates (μ) are 0.0053 and 0.0044 for uninduced and induced PatoL-OG241 in *E. coli* Nissle 1917, and 0.0042 and 0.0035 for uninduced and induced PatoL-LOG241 in *E. coli* Nissle 1917, respectively. Flow cytometry showed that the bacterial biosensors exhibited acetoacetate inducibility by an increase in $\log_{10}$(RFU) of >100-fold for PatoL-OG241 in *E. coli* DH5α (B) and >10-fold for PatoL-LOG241 in *E. coli* DH5α (D) after 16 hours in culture compared to uninduced cultures. Similar to the low copy sensors in *E. coli* DH5α, induced low copy sensors in *E. coli* Nissle 1917 result in two subpopulations with different RFU values.

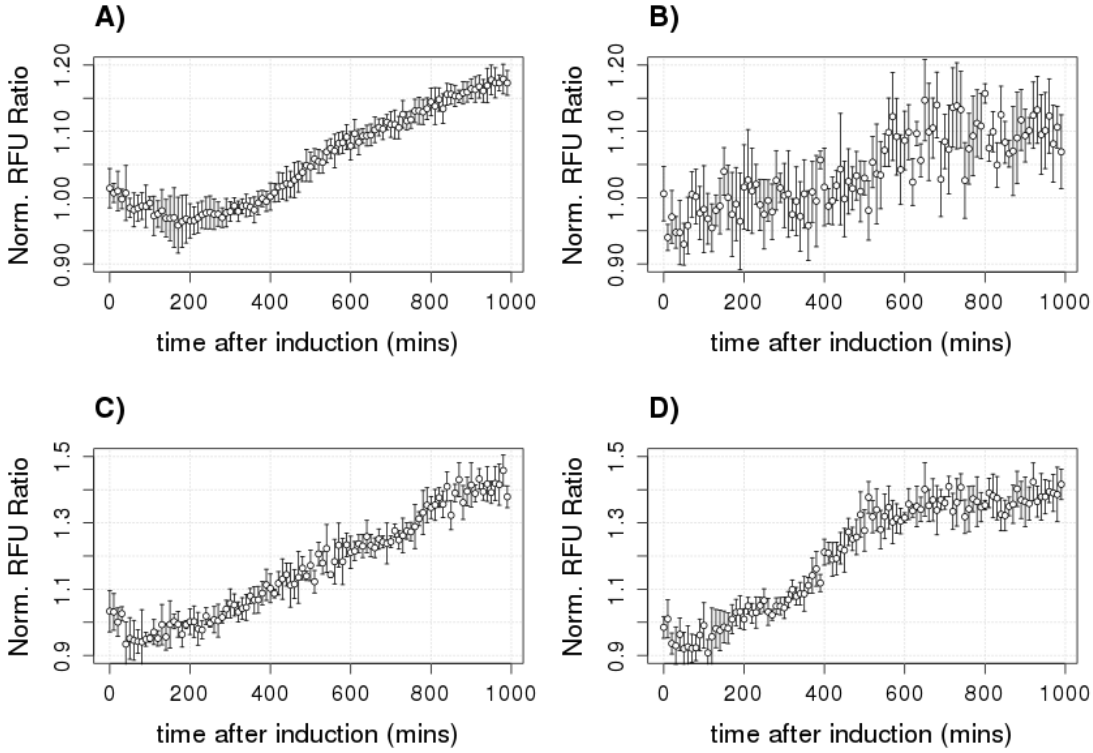

Figure 6: Time series plots of normalized RFU ratios of induced and uninduced acetoacetate bacterial sensors. PatoL-OG241 *E. coli* DH5α (A) show a more distinct induction as compared to PatoL-LOG241 in *E. coli* DH5α (B). The normalized RFU ratio of PatoL-LOG241 in *E. coli* Nissle 1917 (D) reaches a maximum induction more quickly compared to PatoL-OG241 in *E. coli* Nissle 1917 (C). *E. coli* Nissle 1917 biosensors reached higher normalized RFU induction ratios that *E. coli* DH5α.

References

[1] Wang B, Barahona M, Buck M (2013) *A modular cell-based biosensor using engineered genetic logic circuits to detect and integrate multiple environmental signals.* Biosensors and Bioelectronics 40:368-376.

[2] Voigt C (2006) *Genetic parts to program bacteria.* Current Opinion in Biotechnology 17:548-557.

[3] Rogers JK, Guzman CD, Taylor ND, Raman S, Anderson K, Church GM (2015) *Synthetic biosensors for precise gene control and real-time monitoring of metabolites.* Nucleic Acids Research 43(15):7648-7660.

[4] Zhang F, Carothers JM, Keasling JD (2012) *Design of a dynamic sensor-regulator system for production of chemicals and fuels derived from fatty acids.* Nature Biotechnology 30(4):354-359.

[5] Danino T, Prindle A, Kwong GA, Skalak M, Li H, Allen K, Hasty J, Bhatia SN (2015) *Programmable probiotics for detection of cancer in urine.* Science Translational Medicine 7(289):1-11.

[6] Mimee M, Tucker AC, Voigt CA, Lu TK (2015) *Programming a human commensal bacterium, Bacteroides thetaiotamicron, to sense and respond to stimuli in the murine gut microbiota.* Cell Systems 1:62-71.

[7] Courbet A, Endy D, Renard E, Molina F, Bonnet J (2015) *Detection of pathological biomarkers in human clinical samples via amplifying genetic switches and logic gates.* Science Translational Medicine 7(289):1-10.

[8] Foster KJ, Alberti KGMM, Hinks L, Lloyd B, Postle A, Smythe P, Turnell DC, Walton R (1978) *Blood intermediary metabolite and insulin concentrations after an overnight fast: Reference ranges for adults, and interrelations.* Clinical Chemistry 24(9):1568-1572.

[9] Fery F, Balasse EO (1985) *Ketone body production and disposal in diabetic ketosis: A comparison with fasting ketosis.* Diabetes 34:326-332.

[10] Poggetti RS, Moore EE, Moore FA, Bensard DD, Parsons P, Anders BO, Banerjee A (1992) *Gut and liver coordinated metabolic response following major torso injury.* Journal of Surgical Research 52:27-33.

[11] Neal EG, Chaffe H, Schwartz RH, Lawson MS, Edwards N, Fitzsimmons G, Whitney A, Cross JH (2008) *The ketogenic diet for the treatment of childhood epilepsy: a randomised controlled trial.* Lancet Neurology 7:500-506.

[12] Laffel L (1999) *Ketone bodies: a review of physiology, pathophysiology, and application of monitoring to diabetes.* Diabetes/Metabolism Research and Reviews 15(6):412-426.

[13] Enjalbert F, Nicot MC, Bayourthe C, Moncoulon R (2001) *Ketone bodies in milk and blood of dairy cows: relationship between concentrations and utilization for detection of subclinical ketosis.* Journal of Dairy Science 84:583-589.

[14] DeAngelis KM, Ji P, Firestone MK, Lindow SE (2005) *Two novel bacterial biosensors for detection of nitrate availability in the rhizosphere.* Applied and Environmental Microbiology 71(12):8537-8547.

[15] Kotula JW, Kerns SJ, Shaket LA, Siraj L, Collins JJ, Way JC, Silver PA (2014) *Programmable bacteria detect and record an environmental signal in the mammalian gut.* Proceedings of the National Academy of Sciences 111(13):4838-4843.

[16] Kyriakidis DA, Tiligada E (2009) *Signal transduction and adaptive regulation through partial bacterial two-component systems: the Escherichia coli atoSC paradigm.* Amino Acids 37:443-458.

[17] Pauli G, Overath P (1972) *Ato operon: a highly inducible system for acetoacetate and butyrate degradation in Escherichia coli.* European Journal of Biochemistry 29:553-562.

[18] Overath P, Pauli G, Schairer HU (1969) *Fatty acid degradation in Escherichia coli: An inducible acyl-CoA synthetase, the mapping of old-mutations, and the isolation of regulatory mutants.* European Journal of Biochemistry 7:559-574.

[19] Overath P, Raufuss EM, Stoffel W, Ecker W (1967) *The induction of the enzymes of fatty acid degradation in Escherichia coli.* Biochemical and Biophysical Research Communications 29(1):28-33.

[20] Matta MK, Lioliou EE, Panagiotidis CH, Kyriakidis DA, Panagiotidis CA (2007) *Interactions of the antizyme AtoC with regulatory elements of the Escherichia coli AtoDAEB operon.* Journal of Bacteriology 189(17):6324-6332.

[21] Lioliou EE, Mimitou EP, Grigoroudis AI, Panagiotidis CH, Panagiotidis CA, Kyriakidis DA (2005) *Phosphorylation activity of the response regulator of the two-component signal transduction system AtoS-AtoC in E. coli.* Biochimica et Biophysica Acta 1725:257-268.

[22] Jenkins LS, Nunn WD (1987) *Genetic and molecular characterization of the genes involved in short-chain fatty acid degradation in Escherichia coli: the ato system.* Journal of Bacteriology 169(1):42-52.

[23] Jenkins LS, Nunn WD (1987) *Regulation of the ato operon by the atoC gene in Escherichia coli.* Journal of Bacteriology 169(5):2096-2102.

[24] Chen Z, Guo L, Zhang Y, Walzem RL, Pendergast JS, Printz RL, Morris LC, Matafonova E, Stein X, Kang L, Coulon D, McGuinness OP, Niswender KD, Davies SS (2014) *Incorporation of therapeutically modified bacteria into gut microbiota inhibits obesity.* The Journal of Clinical Investigation 241(8):3391-3406.

[25] Duan F, March JC (2010) *Engineered bacterial communication prevents Vibrio cholerae virulence in an infant mouse model.* Proceedings of the National Academy of Sciences 107(25):11260-11264.

[26] Henkert J, Laass M, Blokhin BM, Bolbot YK, Maydannik VG, Elze M, Wolff C, Schulze J (2007) *The probiotic Escherichia coli strain Nissle 1917 (EcN) stops acute diarrhoea in infants and toddlers.* European Journal of Pediatrics 166:311-318.

[27] Kruis W, Schütz E, Fric P, Fixa B, Judmaier G, Stolte M (1997) *Double-blind comparison of an oral Escherichia coli preparation and mesalazine in maintaining remission of ulcerative colitis.* Alimentary Pharmacology and Therapeutics 11:853-858.

[28] Powers JG, Weigman VJ, Shu J, Pufky JM, Cox D, Hurban P (2013) *Efficient and accurate whole genome assembly and methylome profiling of E. coli.* BMC Genomics 14:675.

[29] Beisel CL, Updegrove TB, Janson BJ, Storz G (2012) *Multiple factors dictate target selection by Hfq-binding small RNAs.* The EMBO Journal 31:1961-1974.

[30] Zwietering MH, Jongenburger I, Rombouts FM, Van't Riet K (1990) *Modeling of the bacterial growth curve.* Applied and Environmental Microbiology 56(6):1875-1881.

[31] Theodorou MC, Theodorou EC, Panagiotidis CA, Kyriakidis DA (2007) *Spermidine triggering effect to the signal transduction through the atoS-atoC/Az two-component system in Escherichia coli.* Biochimica et Biophysica Acta 1770:1104-1114.

[32] Khlebnikov A, Risa O, Skaug T, Carrier TA, Keasling JD (2000) *Regulatable arabinose-inducible gene expression system with consistent control in all cells of a culture.* Journal of Bacteriology 182(24):7029-7034.

[33] Jung SC, Smith CL, Lee KS, Hong ME, Kweon DH, Stephanopoulos G, Jin YS (2010) *Restoration of growth phenotypes of Escherichia coli DH5α in minimal media through reversal of point mutation in purB.* Applied and Environmental Microbiology 76(18):6307-6309.

[34] Yordanov B, Dalchau N, Grant PK, Pedersen M, Emmott S, Haseloff J, Phillips A (2014) *A Computational Method for Automated Characterization of Genetic Components.* ACS Synthetic Biology 3(8):578-588

[35] Hartig F, Calabrese JM, Reineking B, Wiegand T, Huth A (2011) *Statistical inference for stochastic simulation models - theory and application.* Ecoogy Letters 14:816-827.

[36] R Development Core Team (2008) *R: A language and environment for statistical computing.* R Foundation for Statistical Computing, Vienna, Austria. ISBN 3-900051-07-0, www.R-project.org.